Research paper

Available Online at http://www.recentscientific.com

CODEN: IJRSFP (USA)

International Journal of Recent Scientific Research

International Journal of Recent Scientific Research
Vol. 17, Issue, 06, pp.728-735, June 2026

ISSN: 0976-3031

Subject Area : Physics

ELECTROCHEMICAL INVESTIGATION OF HEXAGONAL-LIKE $CuMn_2O_4$ NANOFLAKE ELECTRODES FOR HIGH-PERFORMANCE SUPERCAPACITOR APPLICATIONS

P. Vijayamathubalan[1], S. Sivaraj[2], R. Gunaseelan[2], V. Venkatachalam[3], P. Sutharsan[3], S. Abraham Rajasekar[3]* and S. Selvakumar[1]

[1]PG and Research Department of Physics, Government Arts College (Autonomous), Chennai 600 035, Tamil Nadu, India.
[2]Department of Physics, Pachaiyappa's College for Men, Kanchipuram, 631 501, Tamil Nadu, India
[3]Department of Physics, Sir Theagaraya College, Old Washermanpet, Chennai 600 021, Tamil Nadu, India

DOI: http://dx.doi.org/10.24327/ijrsr.20261706.0133

ARTICLE INFO

Article History:

Received 12th May 2026
Received in revised form 24th May2026
Accepted 20th June 2026
Published online 28th June 2026

Key words:

$CuMn_2O_4$ nanoflakes; Pseudocapacitor; XRD; Optical band gap; SEM; EDS

ABSTRACT

$CuMn_2O_4$ electrode materials with a unique hexagonal morphology for supercapacitor applications were synthesized via the co-precipitation technique along with dual hydroxide treatment. Various characterization techniques, such as powder X-ray diffraction (PXRD), Fourier-transform infrared spectroscopy (FTIR), Ultraviolet-Visible Spectroscopy (UV-vis), Scanning Electron Microscopy (SEM), and Energy-dispersive X-ray analysis (EDS), were employed to assess the synthesized material. The electrochemical performance of the $CuMn_2O_4$ electroactive material was evaluated using a three-electrode technique for supercapacitor applications. The hexagonal morphology of the synthesized material provides ample free space and promotes superior electrochemical performance. Cyclic voltammetry (CV) analysis confirmed the pseudocapacitive behaviour, and the maximum specific capacitance was measured at 507.6 F g^{-1} at a scan rate of 5 mV s^{-1} Electrochemical impedance spectroscopy was used to determine the solution resistance (R_s) and charge transfer resistance (R_{ct}). Overall, the findings suggest that the synthesized $CuMn_2O_4$ electrode material holds great potential for use in high-performance supercapacitor applications.

Copyright© The author(s) 2026,This is an open-access article distributed under the terms of the Creative Commons Attribution License, which permits unrestricted use, distribution and reproduction in any medium, provided the original work is properly cited.

INTRODUCTION

The rapid expansion of modern civilization has led to an ever-increasing demand for energy, but the depletion of fossil fuel reserves and their negative impact on climate change have made it imperative to develop sustainable energy storage technologies [1, 2]. Consequently, supercapacitors have garnered significant attention as a promising and environmentally friendly alternative energy source due to their high power density, rapid charge and discharge rates, and long cycle life [3, 4]. Supercapacitors have been employed in various applications, such as electric vehicles, communications, portable devices, and electrical grids [5, 6]. Numerous types of electrode materials, including carbon-based materials, conducting polymers, and metal oxides, have been used for supercapacitor applications [7]. However, the performance of supercapacitors heavily relies on their electrodes. Electrodes based on metal oxides, particularly transition metal oxides (TMOs) exhibit superior redox activity in pseudocapacitors due to their heterogeneous valence states. Although various metal oxides have been reported for supercapacitor applications, such as NiO [8], CuO [9], ZnO [10], and WO_3 [11] their low electronic conductivity and limited cycling stability hinder their effectiveness. To address this issue, researchers have focused on developing AB_2O_4 spinel-based nanomaterials that exhibit superior electrochemical performance and theoretical capacitance, among the spinels, manganese (Mn)-based TMOs

*Corresponding author: **Dr. S. Abraham Rajasekar**

Associate Professor, Department of Physics,
Sir Theagaraya College, Old Washermanpet,
Chennai 600 021, Tamil Nadu, India

are particularly promising material. Mn-based spinel is a vital group of mixed metal oxides, with the chemical formula MMn_2O_4, where M (divalent cation) and Mn (trivalent cation) occupy tetrahedral and octahedral positions, respectively.

In recent years, $CuMn_2O_4$ spinel has attracted significant research attention in various fields, such as photocatalysis, magnetics, gas sensing, and electrochemistry. It has been identified as an ideal material for supercapacitors due to its low cost, redox properties, and excellent conductivity. The combination of the strong oxidation potential of copper and the electron transport ability of manganese produces $CuMn_2O_4$ with exceptional capacitive performance. For instance, Aouini et al.[12] fabricated a $CuMn_2O_4$ spinel-coated stainless steel mesh electrode using the hydrothermal method, achieving a specific capacitance of 1169.3 F g^{-1} at 1 mVs^{-1}. Sanjabi et al.[13] Prepared crystalline copper manganese oxide containing $CuMn_2O_4$ spinel through the co-electrodeposition method and obtained a specific capacitance value of about 744 F g^{-1} at 10 mVs^{-1}. Moreover, Cheng et al.[14] synthesized $CuMn_2O_4$ hierarchical microspheres using micro/nano $MnCO_3$ precursors and measured specific capacitance of 657 F g^{-1} at 1 Ag^{-1}. Saravanakumar et al.[15] reported that rice-like copper manganese oxide demonstrated a specific capacitance of 577 F g^{-1} at 10 mVs^{-1}. Furthermore, according to Zhang et al.[16] $CuMn_2O_4$ spinel anchored on graphene nanosheets exhibited a specific capacitance of 342 F g^{-1} at a current density of 1 Ag^{-1}. Additionally, Kunwar et al.[17] investigated supercapacitive charge storage properties of $CuMn_2O_4$ nanofibers in alkaline and neutral electrolytes. Various methods can be used to prepare metal oxide nanoparticles, including hydrothermal, solid-state, sol-gel, electrochemical, microwave-assisted, co-precipitation, and thermal decomposition. Among these methods, co-precipitation stands out as a simple process, with high purity, and requires no high pressures or temperatures. It also allows for easy control of particle size, crystal structure, and morphology [18,19]. The current research work aimed to synthesize $CuMn_2O_4$ using the co-precipitation method with NaOH and KOH solutions. Various physicochemical properties of the synthesized material were analyzed to understand its characteristics. The electrochemical performance of the obtained $CuMn_2O_4$ electrodes was thoroughly investigated to evaluate their potential for use in supercapacitor applications. Furthermore, we compared the electrochemical parameters obtained from this study with those previously reported in the literature to gain a better understanding of the synthesized material.

EXPERIMENTAL SECTION

Material Synthesis

To prepare the solution, 1 g of $CuCl_2 \cdot 2H_2O$ and 2 g of $MnCl_2.4H_2O$ were added to 50 ml of double distilled (DD) water and magnetic stirred for 30 minutes to form a turquoise-coloured solution, referred to as solution A. Next, solution B was prepared by dissolving 1 g of NaOH and 1 g of KOH in 50 ml of DD water and stirring for 30 minutes. The resulting transparent solution was slowly added dropwise to Solution A while continuing to stir the mixture. Over time, a dark mustard-coloured (brownish) solution formed. The stirring was stopped after 6 hours, and the brown residue settled at the bottom of the beaker. After collecting the sediment, the precipitate was washed several times in DD water and ethanol, then dried overnight in a hot air oven at 100°C. The resulting dried sample was ground into a powder using a mortar and subjected to post-calcination at 450°C for 5 hours. **Fig. 1.** illustrates the schematic diagram of the synthesis process for $CuMn_2O_4$ Nanoflakes.

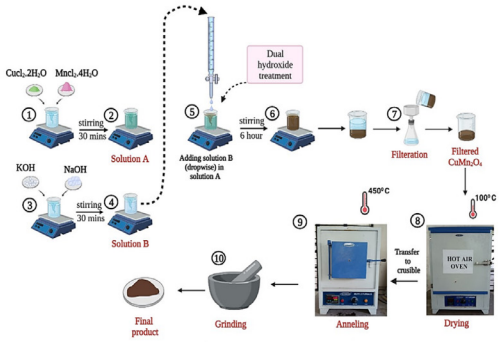

Fig. 1. Schematic illustration of synthesis technique for dual hydroxide treated $CuMn_2O_4$ nanoflakes.

Characterization of $CuMn_2O_4$ material

Powder X-ray diffraction (PXRD) was performed using a Bruker D8 Advance diffractometer with CuKα radiation to determine the crystal structure. Fourier-transform infrared (FTIR) spectroscopy was conducted using a Perkin Elmer Spectrum Two spectrometer analyzer to study the molecular vibrations of the sample. The morphology of the $CuMn_2O_4$ sample was imaged using an Emcraft Genesis 1100 scanning electron microscope (SEM) to visualize the surface and shape. The optical properties of the sample were evaluated by monitoring its UV-Vis absorption spectrum using a Perkin Elmer Lambda 35 instrument, ranging from 190 nm to 1100 nm. The elemental composition of the sample was analyzed using energy-dispersive X-ray spectroscopy (EDS) with a BRUKER nano, GmbH, D-12489 (Germany) instrument. Lastly, electrochemical techniques were employed to study the electrochemical properties of the sample using a SAS Origalys Electrochem electrochemical workstation.

Fabrication of working electrode and electrochemical test

The electrochemical performance of $CuMn_2O_4$ nanostructures was evaluated through various analyses such as cyclic voltammetry (CV), galvanostatic charge-discharge (GCD), and electrochemical impedance spectroscopy (EIS). To prepare the working electrode, graphite paper was utilized as a current collector, which underwent cleaning with DI water and acetone. The active material, along with conducting and binding agents, were blended together in a ratio of 80:10:10 (by weight %), respectively. This mixture was then ground together and dissolved in N-methyl-2-pyrrolidone (NMP) to make the electrode slurry, which was subsequently coated onto graphite paper. The electrochemical analysis was conducted using a three-electrode setup consisting of a platinum wire for the counter electrode, Ag/AgCl for the reference electrode, and $CuMn_2O_4$-coated graphite paper for the working electrode.

The $CuMn_2O_4$ electrode was evaluated using cyclic voltammetry at various scanning rates ranging from 5 to 100 mV s^{-1} within a potential window of 0.0 to 0.5 V. Charge-

discharge technique was recorded at different current densities from 0.5 to 10 Ag^{-1}. Electrochemical impedance spectroscopy was carried out at frequencies ranging from 0.01 Hz to 100 kHz. The specific capacitances of the synthesized $CuMn_2O_4$ electrode were determined using CV and GCD techniques.

RESULTS AND DISCUSSION

Powder X-ray Diffraction studies (PXRD)

The phase purity and crystallinity of the $CuMn_2O_4$ material after calcination was analyzed using a powder X-ray diffractometer, and the obtained diffraction pattern is presented in **Fig. 2.** with a 2θ range of 5°-80°. The diffraction patterns matched perfectly with the standard (JCPDS data file no # 01-074-2422) indicating a cubic structure with an Fd3m space group of $CuMn_2O_4$. The high-intensity peaks in the diffraction pattern suggest a high degree of crystallinity, whereas low-intensity peaks indicate fine grains. The high level of crystallinity and absence of secondary phases indicate good structural integrity of the material, which ensures stable electrochemical performance. A total of twelve characteristic diffraction peaks were observed at 2θ values around18.60°, 30.62°, 35.99°, 37.66°, 43.65°, 47.80°, 54.22°, 57.80°, 63.60°, 66.50°, 72.08°, and 75.10°, which correspond to (111), (220), (311), (222), (400), (331), (422), (511), (400), (531), (620) and (533) crystal planes of $CuMn_2O_4$, respectively. The mean crystalline size (D) of the prepared $CuMn_2O_4$ was calculated using the Debye-Scherer formula,

$$\text{crystalline size } (D) = \frac{K\lambda}{\beta cos\theta} \text{ --------- (1)}$$

Here, K represents the shape factor, λ is the X-ray wavelength obtained from a target, θ is the Bragg's angle, and β refers to the full width at half maximum intensity. The calculated mean crystalline size of the prepared $CuMn_2O_4$ sample was approximately 13.9 nm. This small crystalline size could be beneficial for supercapacitors as it may provide a larger surface area for electrochemical reactions, resulting in higher capacitance. Additionally, the dislocation density (δ) was calculated to understand any imperfections or defects in the crystalline material,

$$\text{dislocation density } (\delta) = {}^{1}/_{D^2}$$

The dislocation density (δ) was calculated to be 5.2×10^{-4} nm^{-2}. Furthermore, the $CuMn_2O_4$ microstrain value was determined using the formula,

$$\text{microstrain } (\varepsilon) = {}^{\beta cos\theta}/_{4}$$

where β is the full width at half maximum intensity. The microstrain value of 0.006773742 was determined. Hooke's law can be applied to calculate microstress (σ=Cε) based on the microstrain value. where C refers to the bulk Young's modulus (1.46 ± 10^{10} N/m^2). The value for the micro stress was calculated to be 98.8966 MPa. The low dislocation density and microstrain value ensure enhanced mechanical stability and resistance to defects, which is ensuring the long-term durability and reliability of the material. Furthermore, micro stress indicates good mechanical strength and ability to withstand external stress for practical applications.

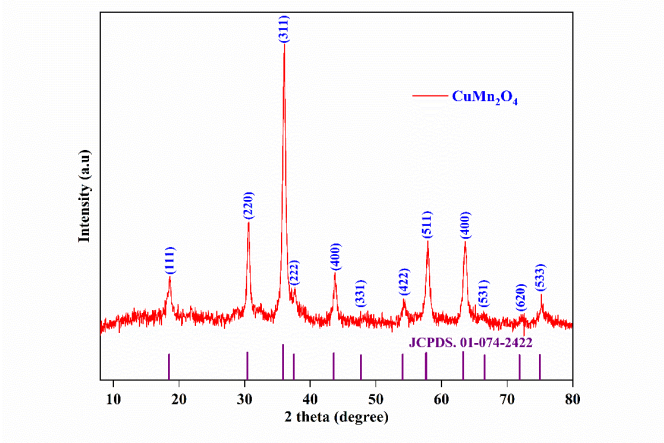

Fig. 2. PXRD of $CuMn_2O_4$ nanoflakes.

Fourier transform infrared spectroscopy analysis (FTIR)

The analysis of functional groups and bonding in the $CuMn_2O_4$ material was carried out by FTIR, as depicted in **Fig. 3.** The presence of the broad peak at 3422 cm^{-1} confirms the existence of OH stretching vibrations, which could be attributed to the surface adsorbed water molecules or hydroxyl groups in the material. The appearance of peaks at 2922 cm^{-1} and 2852 cm^{-1} indicates the presence of C-H stretching vibrations, which could be attributed to the carbon content in the material. Additionally, the peaks at 1632 cm^{-1} and 1113 cm^{-1} correspond to the C-O vibration mode, indicating the presence of carbonates or carboxylic groups. The peak at 1384 cm^{-1} is attributed to the C=O stretching vibrations, indicating the presence of carbonyl groups. From (**inset)** the peaks at 602 cm^{-1} and 529 cm^{-1} correspond to tetrahedral Cu-O and octahedral Mn-O vibrational modes, respectively. These vibrational modes confirm the existence of the Cu-Mn-O bond in the material.

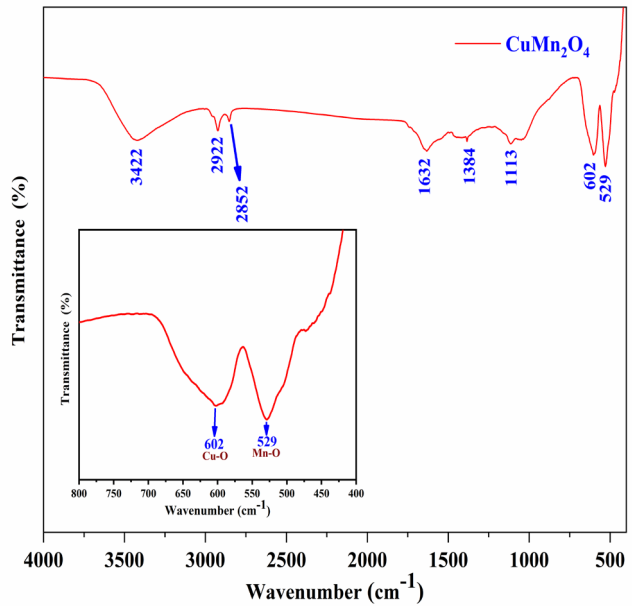

Fig. 3. Infrared spectrum of $CuMn_2O_4$ nanoflakes. (**Inset:** metal-oxygen vibrations in 400-800 cm^{-1} wavenumber region)

The presence of various functional groups in the material, along with the Cu-Mn-O bond, can enhance the electrochemical performance of the material in supercapacitor applications. These functional groups can provide active sites

for surface reactions, while the Cu-Mn-O bond can improve the conductivity and stability of the material. Therefore, the FTIR analysis findings support the suitability of $CuMn_2O_4$ for supercapacitor applications [15],[20].

UV-vis spectroscopy analysis

The $CuMn_2O_4$ sample underwent UV-Vis spectroscopy analysis, and the obtained results are displayed in **Fig. 4.** The spectrum covered a range of 200 to 1100 nm and Tauc's plot **(Inset)** was also obtained. The most prominent absorption peak was observed at 202 nm. Tauc's relation was used to calculate the optical band gap of the sample.

$$(\alpha h\upsilon)^n = A \times (h\upsilon - E_g)$$

Where A stands for a band tailing parameter, hυ denotes photon energy, and α represents the coefficient of absorption. h is the Planks constant (6.626 x 10^{-34} Js). The velocity of light υ = (c/ λ), The light speed is indicated by c (3×10^8 m s^{-1}), and λ is a wavelength. The plot demonstrated a direct allowable band gap type transition, as evidenced by its straight-line nature over a wide range of photon energy. The calculated optical band gap of $CuMn_2O_4$ was found to be 6.5 eV. The absorption peaks observed in the UV-Vis spectrum indicate that $CuMn_2O_4$ can effectively absorb light in the UV range.

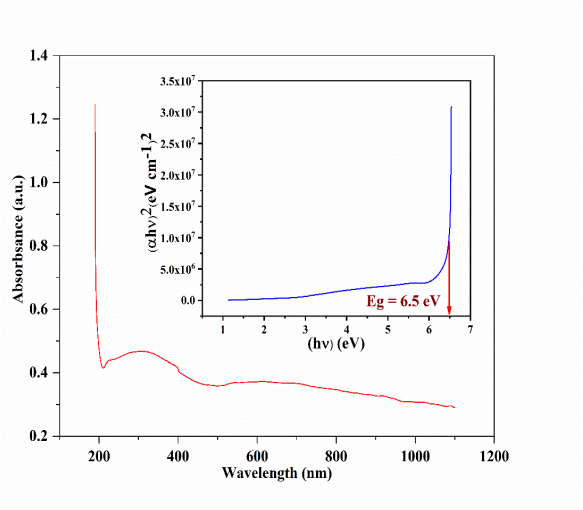

Fig. 4. UV-Visible spectrum

(**Inset:** Energy band gap of $CuMn_2O_4$ nanoflakes)

Morphological studies

SEM analysis was carried out with 100 nm resolutions to investigate the morphology of the prepared $CuMn_2O_4$ material. The obtained SEM images of $CuMn_2O_4$ prepared by dual hydroxide treatment is presented in **Fig. 5(a),** while the corresponding statistical histogram is shown in **Fig. 5(b).** The analysis reveals that the prepared $CuMn_2O_4$ has hexagonal nanoflakes with multigrain agglomerate. The agglomeration in nanoflakes is due to interfacial surface tension created on $CuMn_2O_4$.

The statistical histogram revealed that most of the particles in the $CuMn_2O_4$ sample are within the range of 20 to 40 nm. This size range is highly desirable for supercapacitor applications as it maximizes the surface area of the electrode material. The high surface area of the $CuMn_2O_4$ electrode material allows for more electrolyte ions to be absorbed onto the electrode surface, leading to a higher capacitance. This is further supported by the observation that the hexagonal-like morphology of the electrodes enables them to strongly retain electrolyte ions.

Moreover, The unique morphology of $CuMn_2O_4$ enhances the faradaic effect, which occurs during the charge and discharge process, resulting in efficient charge storage and transfer, as well as high electrochemical performance. These findings suggest that the synthesized $CuMn_2O_4$ sample has significant potential for supercapacitor applications.

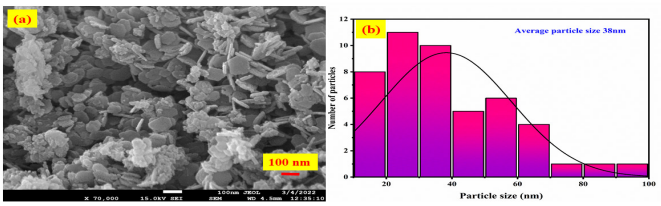

Fig. 5 (a). Surface morphology of $CuMn_2O_4$ at 100 nm and **(b)** its respective statistical histogram for the size distribution

Energy-dispersive X-ray spectroscopy (EDS)

The elemental presence and occupancy ratio in the $CuMn_2O_4$ material were analyzed using EDS. **Fig. 6** displays the EDS spectrum, which confirms the presence of Cu, Mn, and O elements in the $CuMn_2O_4$ material. The EDS spectrum, as shown in **Fig. 6.** confirms the presence of Cu, Mn, and O elements in the material. The observed atomic percentage is very close to the starting stoichiometry, with values of 12.43%, 18.98%, and 68.59% for Cu, Mn, and O, respectively. These results suggest that the synthesis process was successful in producing $CuMn_2O_4$.

The absence of extra foreign substance peaks in the EDS spectrum indicates the high purity of the synthesized $CuMn_2O_4$ sample without any impurities or secondary phases. This observation is consistent with the XRD analysis, which also showed the formation of the $CuMn_2O_4$ pure phase.

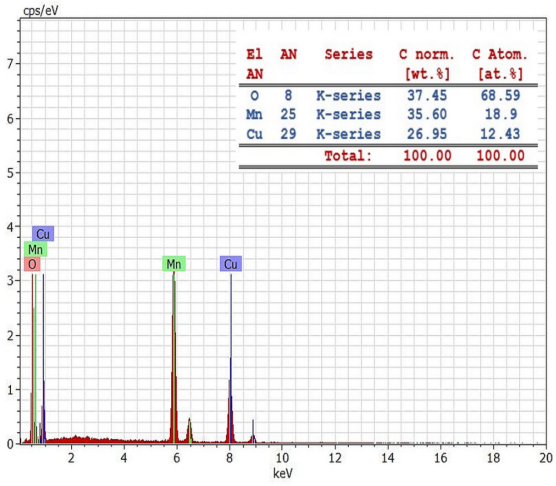

Fig. 6. EDS spectrum of elements Cu, Mn, and O in $CuMn_2O_4$

The high purity and stoichiometry of the synthesized $CuMn_2O_4$ are crucial factors for its potential use in supercapacitor applications. The absence of impurities or secondary phases can prevent any negative effects on the electrochemical performance of the material. The EDS results also suggest that

the synthesized $CuMn_2O_4$ sample can be further evaluated for its electrochemical properties for supercapacitor applications.

ELECTROCHEMICAL STUDIES

Cyclic voltammetry analysis

Cyclic voltammetry (CV) was used to understand the charge storage capacity and charge storage mechanism of the $CuMn_2O_4$ electrode. The electrochemical performance of the $CuMn_2O_4$ electrode was investigated in a 6 M KOH electrolyte at different scan rates from 0 to 0.5 V, and the corresponding CV curves are presented in **Fig. 7(a).** It was observed that the CV curves maintained excellent symmetry at different scan rates, indicating a high-rate capability and strong electrochemical reversibility of the electrode. The CV curves validate the material pseudo-capacitive behaviour and establish the nature of faradic redox reaction. The specific capacitance (C_s) of the working electrode was calculated from the CV curves by using the following formula

$$C_s = \frac{1}{\nu \times m \times (v_a - v_c)} \int I \, dV \text{ ---------- (2)}$$

Where (v_a-v_c) represents the working potential range, ν is the scanning rate, the mass of $CuMn_2O_4$ electro-active material is m, and the integral value of I dV is the area of the CV curve. The results indicated that the $CuMn_2O_4$ electrode material had specific capacitance values of 507.6, 419.6, 308.5, 239.7, 204.24, and 182.04 F g^{-1} for 5, 10, 25, 50, 75, and 100 mV s^{-1}, respectively.

The Dunns method was utilised to verify the electrochemical process responsible for storing electrical energy in an active electrode material. The mechanism of charge storage of electrode material is categorized into two primary components, (i) Faradaic insertion processes that are diffusion-controlled; and (ii) the pseudocapacitive component created by the rapid Faradaic charge transfer processes of an atoms on the surface, and the non-Faradaic process from a double layer of ions adsorption. The total current output (I) observed at a particular potential (V) can be attributed to the cumulative effects of capacitive behaviour ($K_1\nu$) and diffusion-controlled intercalation ($K_2\ \nu^{1/2}$), both of which are influenced by the scan rate (ν) and can be quantified by constants K_1 and K_2. The current (i) obtained from the CV curve follows a power law relation with scan rate,

$$I = a\,\nu^{b} \text{ ---------- (3)}$$

A slope analysis of the log i vs. log ν graph can reveal the value of "b", as shown in **Fig. 7(c).** A slope of 1 on the graph signifies perfect capacitive behaviour, while a b value of 0.5 indicates redox/diffusion-controlled behaviour. For the $CuMn_2O_4$ electrodes, the obtained b value was 0.6, indicating that they displayed mostly redox/diffusion-controlled behaviour with a minor capacitive behaviour. The distribution of the total charges stored between the capacitive and redox mechanisms in electrode materials is shown in equ (4)

$$i(V) = K_1\nu + K_2\nu^{1/2} \text{ ---------- (4)}$$

The percentage of redox and capacitive mechanisms for $CuMn_2O_4$ at various scan rates can be observed in **Fig. 7(d).** The plots indicate that the redox reaction is more effective at slow scan rates as compared to the high scan rates, possibly due to the extended reaction time at lower scan rates. This implies that at higher scan rates, the ability of the electrode to store charge via the diffusion-limited process is reduced. So the specific capacitance value of the electrode also decreases. However, even at the highest scan rate of 100 mV s^{-1}, the electrode exhibits a capacity retention rate of around 36% (in **Fig. 7(b)**, which can be attributed to the unique hexagonal shape of the $CuMn_2O_4$ nanoflakes[21,22].

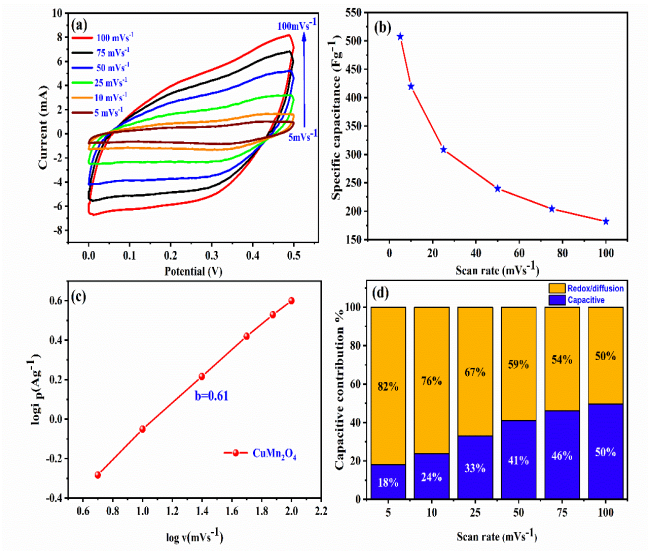

Fig. 7(a). Cyclic voltammograms of $CuMn_2O_4$ at different scan rates, **(b)** Change in specific capacitance with the scan rates, **(c)** b-value from plot of log scan rate vs. log anodic peak current, **(d)** Percentage Contribution of Redox and Capacitive Mechanisms

Galvanostatic Charging-discharging analysis

The galvanostatic charge-discharge curves of $CuMn_2O_4$ samples at various current densities, presented in **Fig. 8 (a).** validate the highly reversible properties of the material, with an almost symmetrical charging and discharging profile. The quasi-triangular symmetry indicates an effective electrochemical pseudocapacitive characteristic of the electrode. These findings corroborate with the CV results, indicating that the electrochemical faradic reaction occurs at the interface between the electrode and electrolyte.

To calculate the specific capacitance of $CuMn_2O_4$, we used the equation:

$$C_s = \frac{I \times t_d}{m \times (v_a - v_c)} \text{ ---------- (5)}$$

Where m is the active mass of the electrode material, t_d is the discharge duration, I is the constant current supplied, and) is the potential difference (0.5 V). We found that at various current densities of 0.5, 1, 2, 3, 4, and 5 A g^{-1}, $CuMn_2O_4$ has specific capacitances of 328.02, 307.94, 243.93, 194.22, 163.57, and 142.37 F g^{-1}, respectively. The capacitance of the electrode material rapidly decreases. However, there is 43% capacity retention even when the current density is increased by a factor of ten. When a supercapacitor undergoes a transition from charging to discharging, the small IR drop is observed in the electrode material, even at high current densities. This indicates high electrical conductivity and low resistance, which are favourable for the performance of supercapacitors. This is because high conductivity can minimize the decline in

capacity and enhance the efficiency and rate capability of the supercapacitors[23].

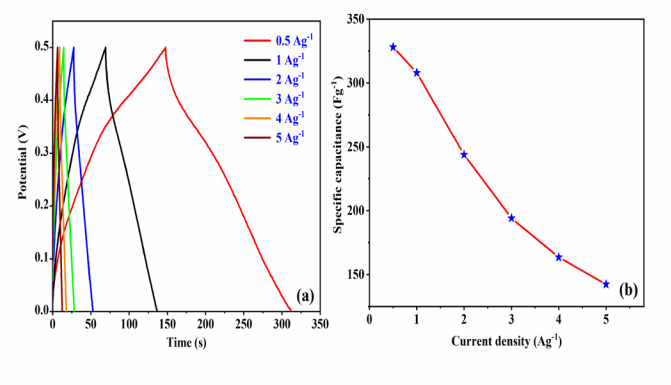

Fig. 8 (a). Galvanostatic charge-discharge curves at different current densities for $CuMn_2O_4$

(b) Change in specific capacitance with the current density

Fig. 8 (b). shows that as the current density increases, Several resistances contribute to the IR drop, such as the resistance of the electrodes, the electrolyte, and the contact between the electrodes and the current collectors. Low internal resistance is highly significant in energy-storing devices as it minimizes energy wastage in the form of unwanted heat during the charging and discharging processes. [24]. The inner active regions of an electrode can be entirely accessed in low current densities with minimal internal resistance. Moreover, the charging and discharging time of the electrode is more prolonged when the current density is lower as compared to when it is higher.

Cycling stability

In evaluating a supercapacitor for practical use, the electrochemical stability and Coulombic efficiency are important considerations. A key requirement for an energy storage device is that it can deliver the same amount of energy under varying operating conditions. Therefore, it is crucial to study the retention of specific capacitance and the Coulombic efficiency at high density [25]. Thus, long-term cycle charge-discharge analysis was conducted on $CuMn_2O_4$ electrode material to investigate cyclic stability. **Fig. 8.** displays the cyclic stability of the electrode under investigation at a current density of 5 A g^{-1} for 5000 consecutive long cycles.

In order to calculate the coulombic efficiency of the $CuMn_2O_4$ electrode, we used the following equation,

$$\eta = (t_d / t_c) \times 100 \text{ ---------- (6)}$$

η the coefficient of coulombic efficiency, t_d the discharge time, and t_c the charging time was determined using the charge-discharge curve. The $CuMn_2O_4$ electrode exhibited a slight decrease in Coulombic efficiency (η) after 5000 cycles but still retained 99.51%, indicating good charge-discharge reversibility. The capacitance retention of the $CuMn_2O_4$ electrode was calculated from the following equation,

$$C_{Ret} = (C_i / C_f) \times 100 \text{---------- (7)}$$

$C_{Ref,}$ the capacitance retention is determined from initial capacitance (C_i) and final capacitance for every 500 consecutive cycles till a maximum of 5000 cycles. The results showed a little drop in capacitance retention during the first 500 cycles. However, after 5000 cycles the capacitance retained 98.77%, which indicates superior cyclic efficiency. The hexagonal-shaped $CuMn_2O_4$ nanoflakes demonstrated enhanced cyclic stability, as the cycling retention rate was near 100% even after 5000 cycles. Moreover, the maximum capacitance retention of $CuMn_2O_4$ nanoflakes was found to be greater than the retention reported in previous studies, indicating the excellent potential of $CuMn_2O_4$ for supercapacitor applications.

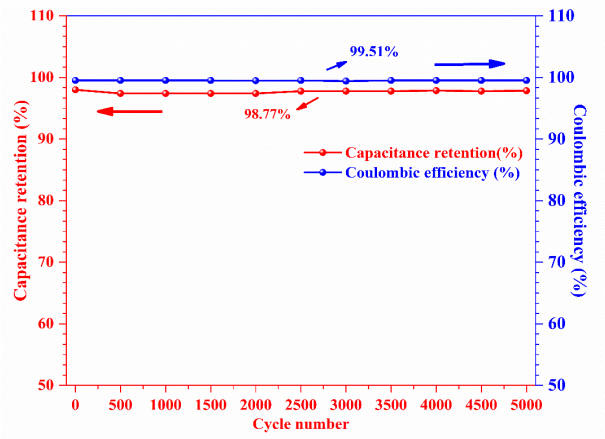

Fig. 9. Coulombic efficiency and capacitance retention during 5000 charge-discharge cycles

Electrochemical impedance spectroscopy analysis

The interface performance between the electrode and electrolyte is an important parameter for evaluating the internal resistance of a supercapacitor, which can be measured using electrochemical impedance spectroscopy (EIS). EIS analysis is a non-destructive approach for assessing electrochemical kinetics in which the electrode is performed using the same aqueous electrolyte (6 M KOH) that was used to get the CV, GCD curves, and cyclic test. The Nyquist plot (**Fig. 10.**) helps to determine the Warburg impedance(W), Charge Transfer Resistance (R_{ct}), and Solution Resistance (R_s) of the $CuMn_2O_4$ electrode. The elements of the equivalent circuit **(inset)** consist of solution resistance (R_s), Warburg resistance (W), charge transfer resistance (R_{ct}), and constant phase element (CPE). CPE is parallel to $R_{ct,}$ also R_s and W were connected in series.

The solution resistance (R_s) incorporates the intrinsic resistance of the electrode, ionic resistance of the electrolyte, and the contact resistance of the electrode-electrolyte interface. The R_s value of $CuMn_2O_4$ is 1.28 Ω at before 5000 cycles and 1.32 Ω is for after 5000 cycles which is a negligible change. The charge transfer resistance (R_{ct}) due to electron transfer has been calculated by taking the diameter of the semicircle. Before the cycle, a tiny semicircle with a diameter of 0.44 Ω (R_{ct}) was noticed;. After the cycle R_{ct} is increased from 0.44 Ω to 0.47 Ω, showing a minimal decrease in capacity for storing ions and hence declining the specific capacitance after 5000 cycles. Low values for R_s, and R_{ct}, are consistent with superior performance, as evidenced by the CV, GCD and cyclic test studies.

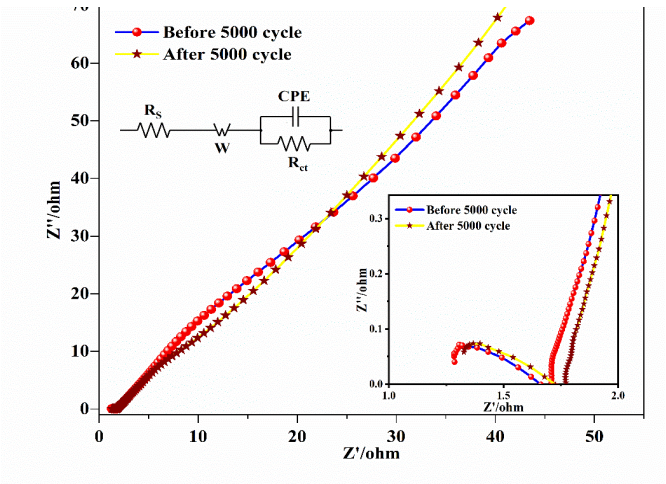

Fig. 10. Nyquist spectrum for $CuMn_2O_4$ electrode in 6M KOH solution

potential of $CuMn_2O_4$ nanoflakes as a promising candidate for energy storage applications. Moreover, the methodology used in this study can be extended to synthesize other metal oxide nanostructures with desired morphologies for electrochemical supercapacitor applications.

Acknowledgment

I thank the ACIC- instrumentation center, St. Joseph's College, Tiruchirappalli-620 002 for material Characterization.

Conflict of interest

There are no conflicts to declare.

Reference

1. S. S and S. V, "Enhanced gravimetric capacitance of CeO_2 by compositing with the hybridized phase of MoS2," *Ionics (Kiel).*, no. i, 2022, doi: 10.1007/s11581-022-04846-3.

Table 1. Comparing $CuMn_2O_4$ specific capacitance value to previous work

Electrode	Synthesis method	Cell configuration	Electrolyte	capacitance (F g^{-1})	Retention (cycle)	Ref.
NiO	hydrothermal	3E	KOH	132 at 5 mVs^{-1}	75% (500)	[8]
CuO	RF magnetron sputtering	3E	PBS	375 F at 1 Ag^{-1}	95% (1000)	[9]
ZnO	Oxidative metal vapor transport method	3E	Na_2SO_4	160.4 at 1 Ag^{-1}	94.3% (1000)	[10]
$CoMn_2O_4$	Electrospinning	3E	NaOH	121 at 5 mVs^{-1}	-	[26]
$CuMn_2O_4$ / RGO	sol-gel method	3E	KOH	342 at 1 Ag^{-1}	75.5% (10000)	[16]
$CuMn_2O_4$	hydrothermal	3E	KOH	571.6 at 0.5 Ag^{-1}	98%	[15]
$CuMnO_2$/ GQD	hydrothermal	2E	KOH	520 at 1 Ag^{-1}	83.3% (5000)	[23]
$CuMn_2O_4$	electrochemical deposition	3E	Na_2SO_4	744 at 10 mVs^{-1}	91% (10000)	[13]
$CuMn_2O_4$ microspheres	Micro/nano sphere $MnCO_3$	3E	KOH	657 at 1 Ag^{-1}	96% (3000)	[14]
$CuMn_2O_4$ coated on SSM	hydrothermal	3E	Na_2SO_4	1169 at 1 mVs^{-1}	-	[12]
$CuMn_2O_4$	Electrospinning	3E	KOH	123 at 0.1 Ag^{-1}	-	[17]
$CuMn_2O_4$	Dual hydroxide treatment	3E	KOH	507.6 at 5 mV s^{-1}	98.77% (5000)	Present study

CONCLUSION

In summary, a hexagonal-like $CuMn_2O_4$ nanoflakes was successfully synthesized via co-precipitation with dual hydroxide treatment. The material was thoroughly characterized using various techniques, including PXRD, FTIR, UV-vis, SEM, and EDS. The electrochemical analyses showed that the $CuMn_2O_4$ electrode had outstanding cycling stability with a coulombic efficiency of 99.51% and capacitance retention of 98.77% after 5000 cycles. The electrode also exhibited a maximum specific capacitance of 507.6 F g^{-1} at a scan rate of 5 mV s^{-1} in a 6M KOH aqueous electrolyte. The unique hexagonal-like morphology of $CuMn_2O_4$ was identified as the key factor in its enhanced electrochemical behaviour, which provides ample free space for energy storage and enhances superior electrochemical performance. These findings demonstrate the

2. X. Sun, Q. Fan, and X. Yin, "Jujube Shell Based-Porous Carbon Composites Double-Doped Doping on Electrochemical Properties," *Materials (Basel).*, vol. 15, no. 21, p. 7532, 2022, doi: https://doi.org/ 10.3390/ma15217532.
3. A. Sahoo and Y. Sharma, "Synthesis and characterization of nanostructured ternary zinc manganese oxide as novel supercapacitor material," *Mater. Chem. Phys.*, vol. 149, pp. 721–727, 2015, doi: 10.1016/j.matchemphys.2014.11.032.
4. S. Suresh and V. Sindhu, "CeO_2/PANI/MoS_2 composite electrode for symmetric supercapacitor application," *J. Indian Chem. Soc.*, vol. 99, no. 10, 2022, doi: 10.1016/j.jics.2022.100727.

5. M. Padmini, P. Elumalai, and P. Thomas, "Symmetric supercapacitor performances of $CaCu_3Ti_4O_{12}$ decorated polyaniline nanocomposite," *Electrochim. Acta*, vol. 292, pp. 558–567, 2018, doi: 10.1016/j.electacta.2018.09.179.
6. S. Kim, S. Lee, and S. Park, "Recent Advanced Supercapacitor : A Review of Storage Mechanisms , Electrode Materials , Modification , and Perspectives," *Nanomaterials*, vol. 12, no. 20, p. 3708, 2022, doi: https://doi.org/10.3390/ nano12203708.
7. Q. Fang, C. Chen, Z. Yang, X. Chen, X. Chen, and T. Liu, "Synthetization and electrochemical performance of pomegranate-like $ZnMn_2O_4$ porous microspheres," *J. Alloys Compd.*, vol. 826, p. 154084, 2020, doi: 10.1016/j.jallcom.2020.154084.
8. S. D. Dhas *et al.*, "Synthesis of NiO nanoparticles for supercapacitor application as an efficient electrode material," *Vacuum*, vol. 181, no. July, p. 109646, Nov. 2020, doi: 10.1016/j.vacuum.2020.109646.
9. G. Mahendra *et al.*, "RF Sputter-Deposited Nanostructured CuO Films for Micro-Supercapacitors," *Appl. Nano*, vol. 2, no. 1, pp. 46–66, 2021, doi: 10.3390/applnano2010005.
10. Q. Luo, P. Xu, Y. Qiu, Z. Cheng, X. Chang, and H. Fan, "Synthesis of ZnO tetrapods for high-performance supercapacitor applications," *Mater. Lett.*, vol. 198, pp. 192–195, Jul. 2017, doi: 10.1016/j.matlet.2017.04.032.
11. V. Lokhande, A. Lokhande, G. Namkoong, J. H. Kim, and T. Ji, "Charge storage in WO_3 polymorphs and their application as supercapacitor electrode material," *Results Phys.*, vol. 12, no. December 2018, pp. 2012–2020, 2019, doi: 10.1016/j.rinp.2019.02.012.
12. S. Aouini, A. Bardaoui, D. M. F. Santos, and R. Chtourou, "Hydrothermal synthesis of $CuMn_2O_4$ spinel-coated stainless steel mesh as a supercapacitor electrode," *J. Mater. Sci. Mater. Electron.*, vol. 33, no. 16, pp. 12726–12733, 2022, doi: 10.1007/s10854-022-08219-4.
13. M. Sheikhzadeh and S. Sanjabi, "Coelectrodeposition of crystalline copper-manganese oxide containing $CuMn_2O_4$ spinel for high energy supercapacitor application," *Synth. Met.*, vol. 278, no. February, p. 116802, 2021, doi: 10.1016/j.synthmet.2021.116802.
14. C. Cheng, Y. Cheng, and G. Lai, "$CuMn_2O_4$ hierarchical microspheres as remarkable electrode of supercapacitors," *Mater. Lett.*, vol. 317, no. February, p. 132102, 2022, doi: 10.1016/j.matlet.2022.132102.
15. B. Saravanakumar, S. Muthu Lakshmi, G. Ravi, V. Ganesh, A. Sakunthala, and R. Yuvakkumar, "Electrochemical properties of rice-like copper manganese oxide ($CuMn_2O_4$) nanoparticles for pseudocapacitor applications," *J. Alloys Compd.*, vol. 723, pp. 115–122, 2017, doi: 10.1016/j.jallcom.2017.06.249.
16. C. Zhang *et al.*, "$CuMn_2O_4$ spinel anchored on graphene nanosheets as a novel electrode material for supercapacitor," *J. Energy Storage*, vol. 34, no. December 2020, p. 102181, 2021, doi: 10.1016/j.est.2020.102181.
17. R. Kunwar *et al.*, "Transformation of Supercapacitive Charge Storage Behaviour in a Multi elemental Spinel $CuMn_2O_4$ Nanofibers with Alkaline and Neutral Electrolytes," *Adv. Fiber Mater.*, vol. 3, no. 4, pp. 265–274, 2021, doi: 10.1007/s42765-021-00083-x.
18. J. Theerthagiri *et al.*, "Synthesis of Hierarchical Cobalt Phosphate Nanoflakes and Their Enhanced Electrochemical Performances for Supercapacitor Applications," *ChemistrySelect*, vol. 2, no. 1, pp. 201–210, 2017, doi: 10.1002/slct.201601628.
19. C. Huang *et al.*, "High-performance supercapacitor based on graphene oxide through in-situ polymerization and co-precipitation method," *J. Alloys Compd.*, vol. 829, p. 154536, 2020, doi: 10.1016/j.jallcom.2020.154536.
20. Y. Gao *et al.*, "$CuMn_2O_4$Spinel Nanoflakes for Amperometric Detection of Hydrogen Peroxide," *ACS Appl. Nano Mater.*, vol. 4, no. 7, pp. 6832–6843, 2021, doi: 10.1021/acsanm.1c00898.
21. Q. Jiang, N. Kurra, M. Alhabeb, Y. Gogotsi, and H. N. Alshareef, "All Pseudocapacitive MXene-RuO_2 Asymmetric Supercapacitors," *Adv. Energy Mater.*, vol. 8, no. 13, pp. 1–10, 2018, doi: 10.1002/aenm.201703043.
22. M. Aftabuzzaman, C. K. Kim, T. Kowalewski, K. Matyjaszewski, and H. K. Kim, "A facile route to well-dispersed Ru nanoparticles embedded in self-templated mesoporous carbons for high-performance supercapacitors," *J. Mater. Chem. A*, vol. 7, no. 35, pp. 20208–20222, 2019, doi: 10.1039/c9ta06571g.
23. M. Ashourdan, A. Semnani, F. Hasanpour, and S. E. Moosavifard, "Synthesis of CuMnO2/graphene quantum dot nanocomposites as novel electrode materials for high performance supercapacitors," *J. Energy Storage*, vol. 36, p. 102449, 2021, doi: 10.1016/j.est.2021.102449.
24. A. A. Ensafi, N. Ahmadi, B. Rezaei, A. Abdolmaleki, and M. Mahmoudian, "A new quaternary nanohybrid composite electrode for a high-performance supercapacitor," *Energy*, vol. 164, pp. 707–721, 2018, doi: 10.1016/j.energy.2018.09.031.
25. B. Bhujun, M. T. T. Tan, and A. S. Shanmugam, "Study of mixed ternary transition metal ferrites as potential electrodes for supercapacitor applications," *Results Phys.*, vol. 7, no. May, pp. 345–353, 2017, doi: 10.1016/j.rinp.2016.04.010.
26. S. Alkhalaf *et al.*, "Electrochemical Energy Storage Performance of Electrospun $CoMn_2O_4$ Nanofibers," *J. Alloys Compd.*, vol. 692, pp. 59–66, 2016, doi: 10.1016/j.jallcom.2016.09.005.

How to cite this article:

Vijayamathubalan et al. (2026). Electrochemical Investigation of Hexagonal-like $CuMn_2O_4$ Nanoflake Electrodes for High-Performance Supercapacitor Applications. *Int J Recent Sci Res*.17(06), pp.728-735.